

Fe I oscillator strengths for the Gaia-ESO survey

M. P. Ruffoni,¹★ E. A. Den Hartog,² J. E. Lawler,² N. R. Brewer,² K. Lind,³
G. Nave⁴ and J. C. Pickering¹

¹Blackett Laboratory, Imperial College London, London SW7 2BW, UK

²Department of Physics, University of Wisconsin, Madison, WI 53706, USA

³Institute of Astronomy, University of Cambridge, Cambridge CB3 0HA, UK

⁴National Institute of Standards and Technology, Gaithersburg, MD 20899-8422, USA

Accepted 2014 April 17. Received 2014 April 11; in original form 2014 March 26

ABSTRACT

The Gaia-ESO Public Spectroscopic Survey (GES) is conducting a large-scale study of multi-element chemical abundances of some 100 000 stars in the Milky Way with the ultimate aim of quantifying the formation history and evolution of young, mature and ancient Galactic populations. However, in preparing for the analysis of GES spectra, it has been noted that atomic oscillator strengths of important Fe I lines required to correctly model stellar line intensities are missing from the atomic data base. Here, we present new experimental oscillator strengths derived from branching fractions and level lifetimes, for 142 transitions of Fe I between 3526 and 10 864 Å, of which at least 38 are urgently needed by GES. We also assess the impact of these new data on solar spectral synthesis and demonstrate that for 36 lines that appear unblended in the Sun, Fe abundance measurements yield a small line-by-line scatter (0.08 dex) with a mean abundance of 7.44 dex in good agreement with recent publications.

Key words: atomic data – line: profiles – methods: laboratory – techniques: spectroscopic.

1 INTRODUCTION

The Gaia-ESO Public Spectroscopic Survey (GES) is currently taking place at the European Southern Observatory (ESO), employing the Fibre Large Array Multi Element Spectrograph (FLAMES) instrument at the Very Large Telescope facility. Its aim is to obtain high-quality spectroscopy of some 100 000 stars from all major components of the Milky Way to quantify the ‘kinematic multi-chemical element abundance distribution functions of the Milky Way bulge, the thick disc, the thin disc, and the halo stellar components, as well as a very significant sample of 100 open clusters (Gilmore et al. 2012). Over the course of the survey, chemical abundances will be measured for alpha and iron-peak elements in all stars with visual magnitude less than 19. These data will probe stellar nucleosynthesis by examining nuclear statistical equilibrium and the alpha-chain. Ultimately, the abundances and radial velocities will be combined with high-precision position and proper motion measurements from the European Space Agency’s *Gaia* mission, to ‘quantify the formation history and evolution of young, mature and ancient Galactic populations’ (Perryman et al. 2001). Gilmore et al. (2012) also state that ‘Considerable effort will be invested in abundance calibration and ESO archive re-analysis to ensure maximum future utility’.

To achieve these high-level aims, it is vital that fundamental atomic data be available for lines in the GES spectral range: 4800–6800 Å for measurements with the high-resolution FLAMES Ultraviolet and Visual Echelle Spectrograph and 8500–9000 Å for measurements with the mid-resolution FLAMES *Giraffe* spectrograph. The availability of absorption oscillator strengths, f (usually used as the $\log(gf)$, where g is the statistical weight of the lower level), is particularly important for the correct modelling and analysis of stellar line intensities; especially so for abundant elements such as iron, which is also used to infer fundamental stellar parameters.

However, in preparing a list of iron lines to be targeted during the analysis of GES spectra, the GES line list team noted that of 449 well-resolved lines of neutral iron (Fe I) expected to be visible with sufficient signal-to-noise ratio, only 167 have published $\log(gf)$ values measured in the laboratory with uncertainties below 25 per cent. Experimental $\log(gf)$ values with large uncertainties (greater than 50 per cent in many cases) were available for an additional 162 lines. For the final 120 lines, no experimental $\log(gf)$ values were available at all. A similar observation was made by Bigot & Thévenin (2006) for lines of interest to the *Gaia* mission.

As a result of this inadequacy in the atomic data base, and similar inadequacies observed by other astronomers (see Ruffoni et al. 2013 and Pickering et al. 2011 for example), we have undertaken a new study of the Fe I spectrum with the aim of providing accurate $\log(gf)$ values for lines of astrophysical significance. In Section 3 of this

★E-mail: m.ruffoni@imperial.ac.uk

paper, we report accurate $\log(gf)$ values for 142 Fe I lines, 64 of which have been measured experimentally for the first time. The $\log(gf)$ values of at least 38 of these lines are urgently needed for the GES survey.

2 EXPERIMENTAL PROCEDURE

Typically, $\log(gf)$ values are obtained in the laboratory from measurements of atomic transition probabilities, A (Thorne, Litzén & Johansson 2007)

$$\log(gf) = \log[A_{ul} g_u \lambda^2 \times 1.499 \times 10^{-14}], \quad (1)$$

where the subscript u denotes a target upper energy level, and ul , a transition from this level to a lower level, l , that results in emission of photons of wavelength λ (nm). g_u is the statistical weight of the upper level. The A_{ul} values are found by combining experimental branching fractions, BF_{ul} , with radiative lifetimes, τ_u (Huber & Sandeman 1986)

$$A_{ul} = \frac{\text{BF}_{ul}}{\tau_u}; \tau_u = \frac{1}{\sum_l A_{ul}}. \quad (2)$$

The BF_{ul} for a given transition is the ratio of its A_{ul} to the sum of all A_{ul} associated with u . This is equivalent to the ratio of observed relative line intensities in photons s^{-1} for these transitions

$$\text{BF}_{ul} = \frac{A_{ul}}{\sum_l A_{ul}} = \frac{I_{ul}}{\sum_l I_{ul}}. \quad (3)$$

This approach does not depend on any form of equilibrium in the population distribution over different levels, but it is essential that all significant transitions from u be included in the sum over l .

The BFs measured for this work were extracted from Fe I spectra acquired by Fourier transform (FT) spectroscopy, as described in Section 2.1. The radiative lifetimes required to solve equation (2) were obtained through laser-induced fluorescence (LIF), and are discussed in Section 2.2.

2.1 Branching fraction measurements

The BFs reported here were obtained from Fe I emission line spectra measured in two overlapping spectral ranges between 8200 and 35 500 cm^{-1} (between 1220 and 282 nm), labelled A and B in Table 1.

Spectrum A was measured between 8200 and 25 500 cm^{-1} (3920.5 and 12 191.8 Å) on the 2 m FT spectrometer at the National Institute of Standards and Technology (NIST; Nave, Sansonetti & Griesmann 1997). The Fe I emission was generated from an iron cathode mounted in a water cooled hollow cathode lamp (HCL) running at a current of 2.0 A in a Ne atmosphere of 370 Pa pressure. The response of the spectrometer as a function of wavenumber was obtained by measuring the spectrum of a calibrated tungsten (W)

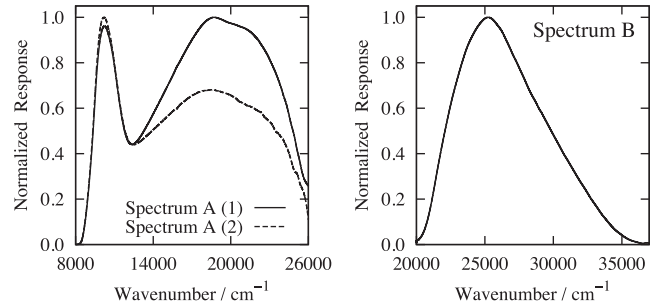


Figure 1. Instrument response functions used to intensity calibrate the two FT spectra listed in Table 1.

halogen lamp with spectral radiance known to ± 1.1 per cent between 250 and 2400 nm. W lamp spectra were acquired both before and after measurements of the Fe/Ne HCL spectrum to verify that the spectrometer response remained stable.

220 individual Fe/Ne HCL spectra were acquired over two days and co-added to improve the signal-to-noise ratio of weak lines. However, due to different detector configurations being used on each day, the spectrometer response function varied significantly between the two. As a result, the files Fe080311.001 to .003 (containing 110 spectra, acquired with a Si photodiode on each output of the FT spectrometer) were co-added and intensity calibrated using the spectral response function labelled ‘Spectrum A (1)’ in Fig. 1, while Fe080411_B.001 to .003 (containing the remaining 110 spectra, acquired with a single Si photodiode mounted on the unbalanced output of the FT spectrometer) were co-added and calibrated using the response function labelled ‘Spectrum A (2)’. These response functions were obtained with the aid of the FAST package (Ruffoni 2013). The two intensity-calibrated line spectra were then themselves co-added to produce the final spectrum.

Spectrum B was measured between 20 000 and 35 500 cm^{-1} (2816.1 and 4998.6 Å) on the Imperial College VUV spectrometer (Thorne 1996), which is based on the laboratory prototype designed by Thorne et al. (1987). The Fe emission was generated from an iron cathode mounted in a new HCL designed and manufactured at Imperial College London (IC). The lamp was operated at 700 mA in a Ne atmosphere of 170 Pa pressure to provide reasonable signal-to-noise ratio in the weaker lines while avoiding self-absorption effects in the stronger lines.

The spectrometer response function for spectrum B is also shown in Fig. 1, and was again obtained from a calibrated W lamp, measured before and after each Fe/Ne HCL measurement. Uncertainties in the relative spectral radiance of the W lamp used at IC, and calibrated by the National Physical Laboratory, do not exceed ± 1.4 per cent between 410 and 800 nm, and rise to ± 2.8 per cent at 300 nm.

Table 1. FTS spectra taken for BF measurements.

Spectrum	Wavenumber ^a range (cm^{-1})	Detector	Filter	Resolution (cm^{-1})	Spectrum filename ^b
A (NIST)	8200–25 500	Si photodiode	None	0.02	Fe080311.001 to .003; Fe080411_B.001 to .003 (220 co-adds)
B (IC)	20 000–35 500	Hammamatsu R11568 PMT	Schott BG3	0.037	Fe130610.002 to .047 (96 co-adds)

Note. The identification of commercial products does not imply recommendation or endorsement by the NIST, nor does it imply that the items identified are necessarily the best available for the purpose.

^aThe equivalent wavelength ranges are: spectrum A: $\lambda = 3920.5$ – $12\,191.8$ Å, spectrum B: $\lambda = 2816.1$ – 4998.6 Å.

^bThe named spectra were co-added to improve the signal-to-noise ratio of weak lines.

Many of the upper energy levels studied here are linked to transitions that produced spectral lines contained entirely within the range of either spectrum A or B. In these cases, all BFs pertaining to those levels were derived from a single spectrum. Where lines associated with a given upper level spanned both spectra, their intensities were put on a common relative scale by comparing the intensity of lines in the overlap region between the two spectra. The process of intensity calibrating overlapping spectra is discussed in detail in Pickering, Johansson & Smith (2001b) and Pickering, Thorne & Perez (2001a).

For each target upper level, the predicted transitions to lower levels were obtained from the semi-empirical calculations of Kurucz (2007). Emission lines from these transitions were then identified in our Fe spectra, and the XGREMLIN package (Nave et al. 1997) used to fit Voigt profiles to those that were observed above the noise limit. The residuals from each fit were examined to ensure that the observed line profiles were free from self-absorption and not blended with other features.

The spectra and fit results from XGREMLIN were then loaded into the FAST package (Ruffoni 2013), where the BFs for each observed target line were measured. Lines which were too weak to be observed – typically those predicted by Kurucz (2007) to contribute less than 1 per cent of the total upper level BF – were not considered, as were lines that were either blended or outside the measured spectral range. Their predicted contribution to the total BF was assigned to a ‘residual’ value, which was used to scale the sum over l of the measured line intensity, I_{ul} , in equation (3).

The calculation of experimental uncertainties in BFs measured by FT spectroscopy with FAST has been discussed in our recent papers (Ruffoni 2013; Ruffoni et al. 2013). The uncertainty in a given BF, ΔBF_{ul} , is

$$\left(\frac{\Delta\text{BF}_{ul}}{\text{BF}_{ul}}\right)^2 = (1 - 2\text{BF}_{ul}) \left(\frac{\Delta I_{ul}}{I_{ul}}\right)^2 + \sum_{j=1}^n \text{BF}_{uj}^2 \left(\frac{\Delta I_{uj}}{I_{uj}}\right)^2, \quad (4)$$

where I_{ul} is the calibrated relative intensity of the emission line associated with the electronic transition from level u to level l , and ΔI_{ul} is the uncertainty in intensity of this line due to its measured signal-to-noise ratio and the uncertainty in the intensity of the standard lamp. From equation (2), it then follows that the uncertainty in A_{ul} is

$$\left(\frac{\Delta A_{ul}}{A_{ul}}\right)^2 = \left(\frac{\Delta\text{BF}_{ul}}{\text{BF}_{ul}}\right)^2 + \left(\frac{\Delta\tau_{ul}}{\tau_{ul}}\right)^2, \quad (5)$$

where $\Delta\tau_{ul}$ is the uncertainty in our measured upper level lifetime. Finally, the uncertainty in $\log(gf)$ of a given line is

$$\Delta \log(gf) = \log\left(1 + \frac{\Delta A_{ul}}{A_{ul}}\right). \quad (6)$$

2.2 Upper level radiative lifetimes

Radiative lifetimes are measured to ± 5 per cent using time-resolved LIF on an atomic beam of iron atoms. A diagram of the apparatus is shown in O’Brian et al. (1991). The beam is produced by sputtering iron atoms in a hollow cathode discharge. The electrical discharge is operated in ≈ 50 Pa argon gas. A DC current of ≈ 30 mA maintains the discharge between ≈ 10 A, 10 μs duration pulses at 30 Hz repetition rate. The hollow cathode, which is lined with a foil of pure iron, is closed on one end except for a 1 mm hole which is flared on one side to act as a nozzle. Energetic argon ions accelerated through the cathode fall potential efficiently sputter the iron from

the surface of the cathode. The iron atoms (neutral as well as singly ionized) are differentially pumped through the nozzle amidst a flow of argon gas into a low-pressure (10^{-2} Pa) scattering chamber. This ‘beam’ is slow (neutrals are moving $\sim 5 \times 10^4$ cm s $^{-1}$ and ions somewhat faster) and weakly collimated.

Measurement of the odd-parity level lifetime required single-step laser excitation. In this technique, the atomic beam is intersected at right angles by a single beam from a nitrogen laser-pumped dye laser 1 cm below the nozzle. The delay between the discharge pulse and the laser pulse is adjustable, and optimized typically at ~ 20 μs , which corresponds to the average transit time of the iron atoms. The scattering volume is at the centre of a set of Helmholtz coils which zeroes the magnetic field to within ± 2 μT . This very low field ensures that the excited iron atoms do not precess about the Earth’s magnetic field, thus eliminating the potential for Zeeman quantum beats in the fluorescence. The dye laser is tunable over the range 205–720 nm using a large selection of dyes as well as frequency doubling crystals. It has a bandwidth of ~ 0.2 cm $^{-1}$, a half-width duration of ~ 3 ns and, more importantly for this work, terminates completely in a few ns. The laser allows for selective excitation of the level under study, eliminating the problem of cascade from higher-lying levels that plagued earlier, non-selective techniques. The laser is tuned to a transition between the ground state or a low-lying metastable level and the level under study. Identifying the correct transition is non-trivial, particularly for a dense, line rich spectrum such as Fe I and Fe II. The laser is tuned to within ≈ 0.1 nm of the transition by adjusting the angle of the grating, which is the tuning element of the laser, while measuring the wavelength with a 0.5 m monochromator. A LIF spectrum of 0.5–1.0 nm range is then recorded using a boxcar averager by slowly changing the pressure in an enclosed volume surrounding the grating. Pressure scanning provides exceptional linearity and reproducibility. The pressure scanned spectrum is then compared to the published linelist from the NIST data base¹ to correctly identify the line of interest.

Fluorescence is collected in a direction mutually orthogonal to the atomic and laser beams through a pair of fused-silica lenses comprising an $f/1$ optical system. A spectral filter, either a broad-band coloured-glass filter or a narrow-band multilayer dielectric filter, is inserted between the two lenses where the fluorescence is approximately collimated. The filter is chosen to maximize fluorescence throughput while reducing or eliminating scattered laser light and eliminating possible cascade from lower-lying levels. Fluorescence is focused on to the photocathode of an RCA 1P28A photomultiplier tube (PMT) and the PMT signal is recorded using a Tektronix SCD1000 transient digitizer. The bandwidth of the PMT, digitizer and associated electronics is adequate to measure lifetimes down to ~ 2 ns. The lifetimes reported here are in the 10–25 ns range and are well within the bandwidth limits. The characteristics of this PMT, i.e. fast rise time and high spectral response in the UV and visible, are favourable for radiative lifetime measurements.

The digitizer is triggered with the signal from a fast photodiode which is illuminated by light picked off from the nitrogen laser. Recording of the fluorescence by the digitizer is delayed until after the dye laser pulse has completely terminated, making deconvolution of the laser temporal profile and fluorescence signals unnecessary. Each data record consists of an average of 640 fluorescence decays followed by an average of 640 background traces with the

¹ <http://physics.nist.gov/PhysRefData/ASD/index.html>

Table 2. Radiative lifetimes for Fe I levels used to derive the $\log(gf)$ values in Table 3. The uncertainty in both our lifetime measurements and those of O'Brian et al. (1991) was ± 5 per cent.

Configuration	Term	J	Upper level		Intermediate level (cm^{-1})	Laser wavelengths ^a		Observation wavelength ^b (nm)	Our lifetime (ns) ± 5 per cent	Previous lifetime (ns) ± 5 per cent
			(cm^{-1})	(eV)		Step 1 (nm)	Step 2 (nm)			
Radiative lifetime for odd parity Fe I levels using single step excitation.										
3d ⁶ (³ H)4s4p(³ P ^o)	y ¹ G ^o	4	48 702.532	6.038 3441		241.906, 414.341			21.0	
Radiative lifetimes for even parity Fe I levels using two-step excitation.										
3d ⁶ (³ D)4s(⁶ D)5s	e ⁵ D	4	44 677.003	5.539 2422	25 899.987	385.991	532.418	561	15.4	15.6 \pm 0.9 ^c
3d ⁷ (⁴ F)5s	e ³ F	4	47 377.952	5.874 1171	26 140.177	382.444	470.727	490	19.9	
3d ⁷ (⁴ F)5s	e ³ F	4	47 960.937	5.946 3981	26 140.177	382.444	458.151	600	22.1	
3d ⁶ (³ D)4s(⁴ D)5s	e ³ D	3	51 294.217	6.359 6721	26 140.177	382.444	397.438	500	9.9	
3d ⁶ (³ D)4s(⁴ D)5s	g ³ D	3	51 770.554	6.418 7304	26 140.177	382.444	390.052	408	12.1	
3d ⁶ (³ D)4s(⁴ D)5s	e ³ D	1	52 039.889	6.452 1236	26 339.694	385.637	388.992	500	10.4	
3d ⁶ (³ D)4s(⁶ D)4d	e ⁵ P	2	52 067.466	6.455 7907	26 140.177	382.444	385.585	446	14.3	
3d ⁷ (⁴ F)4d	f ³ F	4	54 683.318	6.779 8670	36 686.174	404.581	555.489	570	23.5	
Additional radiative lifetimes from O'Brian et al. (1991).										
3d ⁶ 4s(⁶ D)5s	e ⁷ D	4	43 163.323	5.351 5698		423.59				8.5
						427.12				
3d ⁶ 4s(⁶ D)5s	e ⁷ D	2	43 633.530	5.409 8680		418.70				8.4
						423.36				
3d ⁶ 4s(⁶ D)4d	f ³ F	4	51 461.667	6.380 4332		315.32				12.7

Note: The configuration, term, and energy level data are taken from Nave et al. (1994).

^aLaser wavelengths are from the NIST Atomic Spectra Database (<http://www.nist.gov/pml/data/asd.cfm>).

^bFluorescence was observed through ~ 10 nm bandpass multilayer dielectric filters. The filter angle was adjusted where needed to centre the bandpass at the indicated wavelength.

^cMarek, Richter & Stahnke (1979).

Table 3. Experimental BFs, transition probabilities, and $\log(gf)$ values for the Fe I levels listed in Table 2. Only the first upper level is shown here. The full table is available online in machine readable format.

Lower level (l)	Transition		BF	Δ BF (per cent)	A_{ul} (10^6 s^{-1})	This experiment		Published		Ref.	GES target?
	$\lambda_{\text{air}}(\text{\AA})$	$\sigma_{ul}(\text{cm}^{-1})$				$\log(gf)$	\pm	$\log(gf)$	\pm		
	Level 43 163.323 cm^{-1}		3d ⁶ 4s(⁶ D)5s e ⁷ D ₄			8.5 ns \pm 5 per cent		100 per cent complete			
y ⁵ F ₃ *	11 316.1112	8834.539	0.0010	34.2	0.117	-1.70	0.13				
y ⁵ D ₃ *	10 353.2077	9656.196	0.0004	29.1	0.052	-2.13	0.11				
z ³ F ₄ *	8432.1889	11 856.059	0.0015	19.3	0.178	-1.77	0.08				
z ⁵ D ₄	5792.6238	17 263.334	0.0012	14.3	0.146	-2.18	0.06	-2.23	0.10	O'Brian et al. (1991)	
z ⁷ P ₃	5268.0211	18 982.460	0.0963	0.9	11.334	-0.37	0.02	-0.39	0.03	O'Brian et al. (1991)	
z ⁷ P ₄	5140.8947	19 451.867	0.0793	0.9	9.335	-0.48	0.02	-0.51	0.03	O'Brian et al. (1991)	
z ⁷ F ₃	4986.9382	20 052.384	0.0115	1.5	1.349	-1.34	0.02	-1.33	0.04	O'Brian et al. (1991)	Yes
z ⁷ F ₄	4958.6820	20 166.649	0.1086	0.9	12.776	-0.37	0.02	-0.41	0.03	O'Brian et al. (1991)	Yes
z ⁷ F ₅	4921.8768	20 317.453	0.3082	0.7	36.260	0.07	0.02	0.07	0.03	O'Brian et al. (1991)	Yes
z ⁷ D ₃	4272.3558	23 406.290	0.1559	0.8	18.345	-0.35	0.02	-0.35	0.01	Blackwell et al. (1982)	
z ⁷ D ₄	4237.1298	23 600.882	0.1625	1.0	19.121	-0.34	0.02	-0.34	0.01	Blackwell et al. (1982)	
z ⁷ D ₅	4199.4872	23 812.431	0.0724	0.9	8.516	-0.69	0.02	-0.72	0.01	Blackwell et al. (1982)	
	Residual		0.0012								

laser tuned off-line. The data are divided into an early time and a late time interval for analysis. A linear least-squares fit to a single exponential is performed on the background subtracted fluorescence decay to determine a lifetime for each interval. Comparison of the lifetimes in the two intervals is a sensitive indicator of whether the decay is a clean exponential or whether some systematic effect has rendered it non-exponential. Five of these decay times are averaged together to determine the lifetime. The lifetime of each odd-parity level is measured twice, using two different laser transitions. This redundancy helps to ensure that the transition is classified correctly, free from blends, and is identified correctly in the experiment.

Measurement of the even-parity levels reported here required two-step laser excitation. The introduction of a second laser results in an added layer of complexity in the excitation of the level and timing of the experiment, as well as more stringent requirements for the filtering of the fluorescence. The fluorescence detection, recording and analysis is identical to the one-laser experiment. While it is possible to pump two dye lasers using one nitrogen laser, this limits the power available in either laser beam. Instead, we used two dye lasers each with its own nitrogen laser pump. The delay generator which, in the one laser experiment is used to trigger the laser ~ 20 μs after the discharge pulse, is in this case used to trigger a second dual gate generator that has very precise timing (± 1 ns) between

Table 4. Lines measured in previous studies, or predicted to have a BF greater than 1 per cent, that were omitted from the BF measurements shown in Table 3. Only the first upper level is shown here. The full table is available online in machine readable format.

Lower level (<i>l</i>)	Transition		Published		Ref.	Predicted BF	Reason for omission	Probable blends
	λ_{airul} (Å)	σ_{ul} (cm ⁻¹)	$\log(gf)$	\pm^a				
	Level 44 677.003 cm ⁻¹		3d ⁶ (⁵ D)4s(⁶ D)5s e ⁵ D ₄			15.4 ns \pm 5 per cent	97 per cent complete	
y ⁵ P ₃	12 638.7060	7910.038	-0.774		Kurucz (2007)	0.0107	Outside range	
z ⁷ P ₃	4877.6064	20 496.135	-3.090	E	May et al. (1974)	0.0003	Not observed	
z ⁷ F ₃	4635.6170	21 566.062	-3.530	E	May et al. (1974)	0.0001	Not observed	
z ⁷ D ₃	4011.7113	24 919.974	-2.630	D	May et al. (1974)	0.0015	Not observed	
					Sum	0.0126		

^a Data from May et al. (1974) are given the uncertainty codes ‘D’ and ‘E’ to follow the notation used by Fuhr & Wiese (2006). A letter ‘D’ indicates that the uncertainty is likely to be up to 50 per cent. A letter ‘E’ indicates a probable uncertainty greater than 50 per cent but within a factor of 2 in most cases. All numeric uncertainties are quoted as they appear in the source publication.

its two gates. These gates are used to trigger the two nitrogen lasers which pump the dye lasers. Because the two nitrogen lasers have different thyatron charging and firing mechanisms, there is a substantial amount of timing jitter (approximately ± 20 ns) between the resulting dye laser pulses. This jitter results in some additional shot-to-shot fluctuation in the final measurement as the population in the intermediate level has decayed more or less from its peak. The lifetimes of all the intermediate levels used but one is substantially longer than this jitter (60–85 ns as measured by O’Brian et al. 1991), so the added shot-to-shot noise was not severe. Even the measurement with the short-lived (9.6 ns as measured by O’Brian et al. 1991) intermediate level had only ~ 2 per cent statistical scatter in the final average. The delay between the two lasers is adjusted such that the laser which drives the transition from the intermediate level to the even-parity level being studied (laser 2) arrives on average ~ 20 ns after that which drives a transition between the ground or low-lying metastable level and an intermediate odd-parity level (laser 1). The trigger signal for the boxcar and digitizer was from the fast photodiode illuminated with light from the laser 2 nitrogen laser.

The two lasers are sent through the scattering chamber at slight angles relative to each other, such that they intersect in the viewing volume. Once laser 1 is tuned on to the appropriate transition to drive the intermediate level, it is left there for the duration of the measurement. A narrow-band, multilayer dielectric filter is inserted in the collection optics which completely blocks fluorescence from the intermediate level but transmits fluorescence from the upper level. Laser 2 was tuned on and off the transition to provide the fluorescence and background traces as in the one-step experiment. The fluorescence was observed to go away when either laser 1 or laser 2 was blocked and the other laser was allowed to pass through the system, ensuring that it was indeed from a two-step process. This provides the assurance that the correct lifetime is being measured that a redundant measurement gives in the one-step experiment. Each two-step lifetime was therefore measured only once.

Systematic effects such as Zeeman quantum beats and bandwidth limits are well studied and controlled in the experiment. Another effect, the flight out of view effect, is caused by atoms leaving the viewing volume before fluorescing. This effect is only a problem for long lifetimes, greater than 300 ns for neutrals and greater than 100 ns for ions, and is not a problem for the current set of lifetimes. In addition to understanding and minimizing these systematics, we also regularly measure a set of benchmark lifetimes, to compare our measured values to the known lifetimes. These benchmarks are lifetimes that are either very well known from theoretical calculations, or from an experiment which has significantly smaller and generally

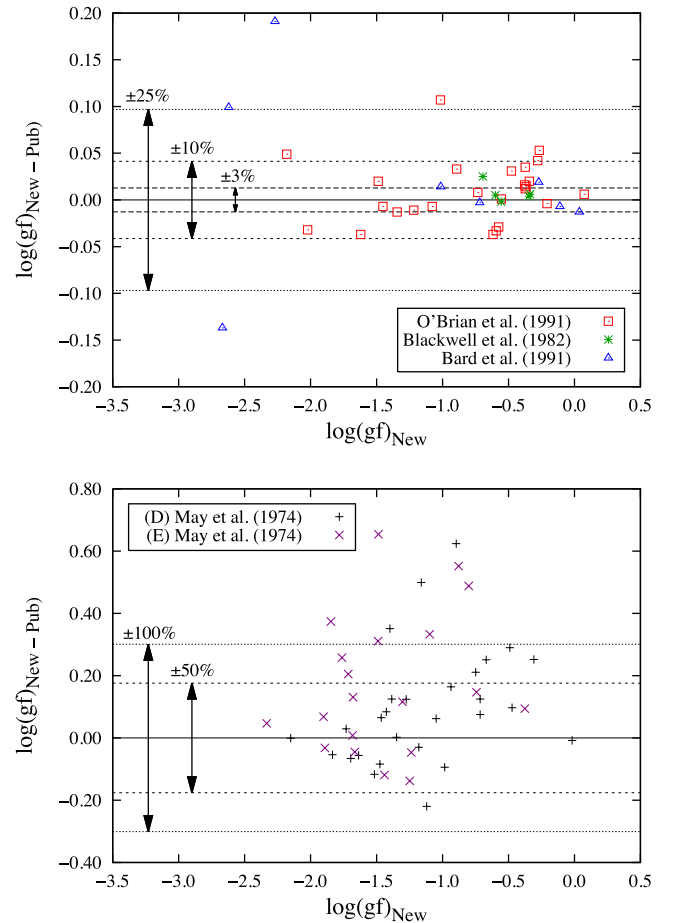


Figure 2. A comparison between the $\log(gf)$ values of this work and those already in the literature. The upper panel shows results from O’Brian et al. (1991), Blackwell et al. (1982) and Bard et al. (1991), which agree well with our new $\log(gf)$ values. The lower pane shows the corrected results from May et al. (1974), which have a considerably lower accuracy.

different systematic uncertainties from our own. For the current set of lifetimes, we measured three benchmarks which approximately bracketed the range of values reported here. These are: $2p^2P_{3/2}$ level of singly ionized Be at 8.8519(8) ns (variational method calculation Yan-C., Tambasco & Drake 1998); the $3p^2P_{3/2}$ level of neutral Na at 16.23(1) ns (accuracy of ≤ 0.1 per cent at 90 per cent confidence level) taken from the recent NIST critical compilation of Kelleher & Podobedova (2008); and the $2p_24p[1/2]_1$ level of neutral Ar

Table 5. Lines from Table 3 selected for solar synthesis.

λ_{air} (Å)	χ_{lower} (eV)	VdW ^a parameter	This experiment		Previously published		Ref.	log [ε(Fe)]	
			log(<i>gf</i>)	±	log(<i>gf</i>)	± ^b		This experiment	Previous work
4423.8408	3.654	933.274	-1.61	0.05	-1.58	D	May et al. (1974)	7.43	7.40
4807.7088	3.368	904.227	-2.15	0.05	-2.15	D	May et al. (1974)	7.56	7.56
5001.8636	3.882	725.240	-0.01	0.02	-0.01	D	May et al. (1974)	7.41	7.41
5022.2355	3.984	742.238	-0.33	0.02	-0.56	D	May et al. (1974)	7.43	7.66
5285.1286	4.435	1046.282	-1.66	0.13	-1.62	E	May et al. (1974)	7.60	7.56
5373.7086	4.473	1044.282	-0.71	0.03	-0.76	D	May et al. (1974)	7.40	7.45
5393.1676	3.241	791.237	-0.72	0.02	-0.72	0.03	Bard et al. (1991)	7.44	7.44
5473.9005	4.154	738.241	-0.72	0.03	-0.79	D	May et al. (1974)	7.48	7.55
5538.5162	4.218	-7.480	-1.54	0.06	-3.24		Kurucz (2007)	7.49	9.19
5615.6439	3.332	794.241	0.04	0.02	0.05	0.03	Bard et al. (1991)	7.45	7.44
5638.2621	4.220	730.235	-0.72	0.02	-0.84	D	May et al. (1974)	7.42	7.54
5717.8329	4.284	758.209	-0.96	0.03	-1.10	D	May et al. (1974)	7.50	7.64
5784.6584	3.397	796.244	-2.67	0.09	-2.53	0.03	Bard et al. (1991)	7.55	7.41
6003.0123	3.882	898.241	-1.10	0.02	-1.12		Kurucz (2007)	7.58	7.61
6056.0047	4.733	1029.286	-0.32	0.03	-0.46		Kurucz (2007)	7.38	7.52
6315.8115	4.076	410.250	-1.63	0.10	-1.61		Kurucz (2007)	7.48	7.47
6400.0012	3.603	802.252	-0.27	0.02	-0.29	0.03	Bard et al. (1991)	7.42	7.44
6627.5448	4.549	754.209	-1.59	0.10	-1.58		Kurucz (2007)	7.57	7.56
6705.1024	4.607	-7.480	-0.87	0.04	-1.39		Kurucz (2007)	7.31	7.83
6725.3572	4.103	897.241	-2.10	0.10	-2.01		Kurucz (2007)	7.36	7.28
6841.3391	4.607	759.267	-0.49	0.03	-0.78	D	May et al. (1974)	7.25	7.54
6843.6560	4.549	736.216	-0.73	0.03	-0.83	D	May et al. (1974)	7.38	7.48
6916.6815	4.154	901.243	-1.28	0.03	-1.40	D	May et al. (1974)	7.46	7.58
6999.8841	4.103	845.244	-1.38	0.03	-1.46	D	May et al. (1974)	7.46	7.54
7007.9701	4.178	903.244	-1.77	0.04	-1.96		Kurucz (2007)	7.37	7.56
7306.5623	4.178	846.244	-1.43	0.03	-1.43		Kurucz (2007)	7.35	7.35
7661.1974	4.256	-7.550	-0.88	0.02	-0.83		Kurucz (2007)	7.52	7.47
8571.8052	5.010	-7.480	-1.11	0.04	-1.41		Kurucz (2007)	7.48	7.78
8610.6120	4.435	-7.550	-1.69	0.04	-2.65		Kurucz (2007)	7.41	8.37
8699.4540	4.956	-7.510	-0.37	0.02	-0.38	0.13	O'Brian et al. (1991)	7.41	7.42
8905.9947	5.064	-7.480	-1.22	0.04	-3.65		Kurucz (2007)	7.45	9.88
8945.1900	5.033	-7.530	-0.23	0.03	-0.23		Kurucz (2007)	7.46	7.46
9103.6375	4.178	-7.540	-2.19	0.05	-1.96		Kurucz (2007)	7.53	7.30
9199.4455	5.033	-7.510	-1.12	0.04	-1.01		Kurucz (2007)	7.30	7.19
9786.6450	4.608	-7.550	-1.84	0.04	-1.68		Kurucz (2007)	7.46	7.30
10 863.5200	4.733	-7.550	-0.90	0.02	-0.90		Kurucz (2007)	7.45	7.45

^aVan der Waals broadening parameter. Values greater than zero were obtained from Anstee, Barklem & O'Mara (ABO) theory (Anstee & O'Mara 1991, 1995) and are expressed in the standard packed notation where the integer component is the broadening cross-section, σ , in atomic units, and the decimal component is the dimensionless velocity parameter, α . Values less than zero are the log of the VdW broadening parameter, γ_6 (rad s⁻¹), per unit perturber number density, N (cm⁻³), at 10 000 K (i.e. log [γ_6/N] in units of rad s⁻¹ cm³). These were used only when ABO data were unavailable. See Gray (2005) for more details.

^bData from May et al. (1974) are given the uncertainty codes 'D' and 'E' to follow the notation used by Fuhr & Wiese (2006). A letter 'D' indicates that the uncertainty is likely to be up to 50 per cent. A letter 'E' indicates a probable uncertainty greater than 50 per cent but within a factor of 2 in most cases. All numeric uncertainties are quoted as they appear in the source publication.

at 27.85(7) ns (beam-gas-laser-spectroscopy; Volz & Schmoranzler 1998). Benchmarks are measured in exactly the same way as the Fe I lifetimes except that the cathode lining is changed in the cases of the Be⁺ and Na measurements. With these benchmarks we are able to quantify and make small corrections for any residual systematic effects ensuring that our final results are well within the stated uncertainty of ±5 per cent. A recent comparison of LIF measurements in Sm II by Lawler et al. (2008) suggests that the ±5 per cent is a conservative estimate of the lifetime uncertainty.

The lifetime results are given in Table 2. A total of one odd-parity and eight even-parity level lifetimes were measured; most for the first time. The even-parity e^5D_4 level at 44 677.003 cm⁻¹ was also measured by Marek et al. (1979) using delayed coincidence detection after laser excitation, and agrees with our lifetime to about ±1 per cent. This good level of agreement is what we have come to expect between modern, laser-based methods.

3 RESULTS

Table 2 lists the Fe I upper levels that were targeted in this study. They were selected because their branches to lower levels produce many spectral lines of interest to the GES survey that currently have either no experimentally measured log(*gf*) value in the literature, or a log(*gf*) known to worse than ±25 per cent. We also included two levels, those at 43 633.530 and 51 461.667 cm⁻¹, for which accurate lifetimes and log(*gf*) values were reported by O'Brian et al. (1991). These served primarily as a means to check the accuracy of log(*gf*) values produced with the aid of the FAST code, but in remeasuring them we were also able to improve upon the experimental uncertainty achieved by O'Brian et al. (1991) and provide log(*gf*) values for a number of weaker branches not included in their paper. Some further lines reported by O'Brian et al. (1991) appear in branches from other upper levels, as do a few lines for which accurate log(*gf*)

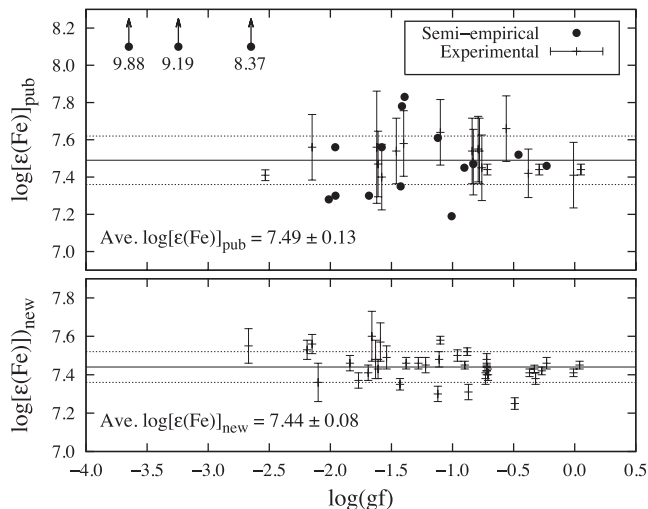


Figure 3. Solar metallicity, $\log[\epsilon(\text{Fe})]$, obtained from the synthesis of individual lines listed in Table 3 using the $\log(gf)$ values from this work, $\log(gf)_{\text{New}}$, and the best previously published values, $\log(gf)_{\text{Pub}}$. Only those lines that appear unblended in the solar spectrum are included. The three points at the top left of the upper pane are discrepant semi-empirical values that lie outside the plotted range at the values shown. They were not included in the calculation of the average $\log[\epsilon(\text{Fe})]_{\text{Pub}}$.

values were reported by Blackwell et al. (1982) and Bard, Kock & Kock (1991). Again, these served as a means to check the accuracy of our results.

Our measured BFs, transition probabilities, and $\log(gf)$ values are listed in Table 3 along with the most accurate $\log(gf)$ values previously available in the literature. The lower level terms, and transition vacuum wavenumbers and air wavelengths were taken from Nave et al. (1994), where possible. For the small number of lines not included in Nave et al. (1994), the transition vacuum wavenumber and air wavelength shown were obtained from our FT spectra by calibrating the measured wavenumber scale to match the calibrated scale used by Nave et al. (1994). These lines are marked in Table 3 by an ‘*’ in the Lower level column.

Table 3 is sorted in order of ascending transition wavenumber, with lines grouped by common upper level energy. For each set of lines, the upper level energy, configuration, term and J value, and measured lifetime are given as a header row. The unobserved ‘residual’ BF, described in Section 2.1, is given in the BF column at the end of each set. The lines that contribute to these residuals are given in Table 4 where they have either been observed in previous studies, or predicted by Kurucz (2007) to contribute more than 1 per cent to the total BF. Reasons for their omission in this study are given.

For 6 of the 11 upper levels (those at 43 633.530, 44 677.003, 47 377.952, 47 960.937, 48 702.532 and 51 294.217 cm^{-1}) the residual BF amounted to less than 5 per cent, and arose solely from lines predicted by Kurucz (2007) to contribute to the total set of branches that were too weak to be observed experimentally. For the remaining five levels (those at 51 461.667 $^{-1}$, 51 770.554 $^{-1}$, 52 039.889, 52 067.446 and 54 683.318 cm^{-1}) a large majority of branches were observed, but at least one stronger line was unavailable due to being unobserved above the spectral noise, blended with another line, or significantly separated in wavenumber from the rest of the branches (which prevents correct intensity calibration). In all cases, the missing BF was taken from previously published values, if they existed, or from Kurucz’s calculations otherwise, as shown in Table 4. Any error in these values will affect the overall normal-

ization of $\log(gf)$ values for the level in question, in turn leading to a systematic error in their value. However, we expect this error to be small, and so have neglected it, for two reasons. First, there is good agreement between our $\log(gf)$ values and those from O’Brian et al. (1991) for branches from the 51 461.667 cm^{-1} level, which has a residual BF of 0.124 (the largest of all levels), and secondly, this residual can be varied by as much as ± 20 per cent without the normalization error exceeding the random uncertainty in $\log(gf)$ of any of the branches.

Lines that are of particular interest for the GES survey are marked in Table 3 in the ‘GES Target?’ column. In some cases the $\log(gf)$ values for these lines have been measured in earlier studies, in which case we have sought to reduce their uncertainty. For lines originally measured by May, Richter & Wichelmann (1974), the quoted published $\log(gf)$ values are the corrected values given by Fuhr & Wiese (2006) in their recent critical compilation of Fe I $\log(gf)$ values. In preparing their compilation, these authors noted that the lifetimes used by May et al. (1974) originate from data produced in the 1960s and early 1970s. Comparing these to the cascade-free LIF lifetimes measured by O’Brian et al. (1991), they found that for 13 energy levels between 52 000 and 57 000 cm^{-1} the lifetimes given by O’Brian et al. (1991) were systematically shorter by about 20 per cent, most likely due to the absence of cascade effects. For levels below 36 000 cm^{-1} , this systematic error vanished. Fuhr & Wiese (2006) therefore corrected the $\log(gf)$ values given by May et al. (1974) for levels above 36 000 cm^{-1} to make them consistent with the lifetime data of O’Brian et al. (1991). For the remaining $\log(gf)$ values, Fuhr & Wiese (2006) found fair agreement with the results of O’Brian et al. (1991) and Blackwell et al. (1982) where they overlapped. However, the scatter was ‘quite large’, suggesting that the uncertainties given by May et al. (1974) should be significantly larger. In Table 3, the uncertainties in $\log(gf)$ values from May et al. (1974) are therefore given as a letter ‘D’ or ‘E’ to follow the notation used by Fuhr & Wiese (2006). A letter ‘D’ indicates that the uncertainty is likely to be up to 50 per cent, whereas an ‘E’ indicates a probable uncertainty greater than 50 per cent, but within a factor of 2 in most cases.

Fig. 2 shows a comparison between our new $\log(gf)$ values and those published previously. The top panel shows the difference between our values and those reported by O’Brian et al. (1991), Blackwell et al. (1982) and Bard et al. (1991). The long dashed, short dashed and dotted horizontal lines indicate uncertainties of ± 2 , ± 10 and ± 25 per cent, respectively, corresponding to uncertainties coded ‘A’, ‘B’ and ‘C’ by Fuhr & Wiese (2006). The work of Blackwell et al. (1982) continues to serve as a gold-standard for Fe I $\log(gf)$ values in the literature. Five lines from their study are also included our work, and the $\log(gf)$ for each agrees within their combined experimental uncertainty of ± 5 per cent. There is also very good agreement with the results of O’Brian et al. (1991) and Bard et al. (1991). 25 of the 29 $\log(gf)$ values from these papers agree within the combined experimental uncertainties with no discernible systematic offset between the published results and our new values. Together, these testify to the general accuracy of our $\log(gf)$ measurements and the accuracy of the FAST code in extracting $\log(gf)$ values from FT spectra.

The lower panel of Fig. 2 shows the difference between our values and the corrected $\log(gf)$ values given by Fuhr & Wiese (2006) for the data reported by May et al. (1974). The dashed and dotted lines this time indicate uncertainties of ± 50 and ± 100 per cent, respectively, which correspond to uncertainties coded ‘D’ and ‘E’ by Fuhr & Wiese (2006). 31 of the 39 corrected $\log(gf)$ values from May et al. (1974) agree with our new values when

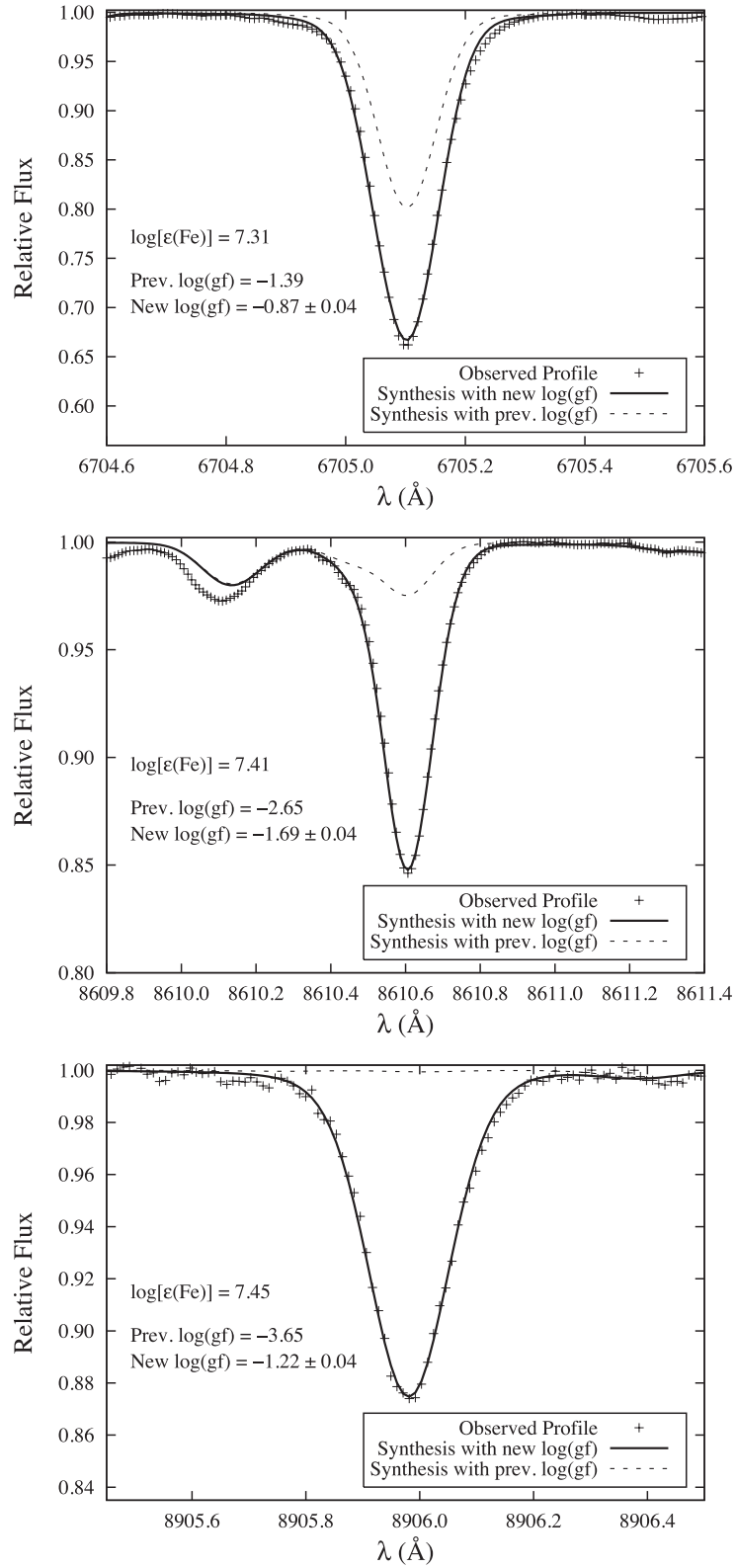


Figure 4. Three examples of lines observed in the solar spectrum and synthesized using both the $\log(\text{gf})$ values from this work and the best previously published values. The solid lines show the synthetic profiles obtained using the $\log(\text{gf})$ values from this work and the quoted values of $\log[\epsilon(\text{Fe})]$. The dashed lines show the synthetic profiles obtained using the same values of $\log[\epsilon(\text{Fe})]$, but adopting the best previously published $\log(\text{gf})$ values, shown in Table 5.

considering the enlarged uncertainties attributed to them by Fuhr & Wiese (2006), but there is considerable scatter in the results, as was also noted by Fuhr & Wiese (2006). There is also a systematic offset of $\log(gf)_{(\text{New-Pub})} = 0.12$ for these lines. Our new $\log(gf)$ values for these lines are accompanied by considerably smaller uncertainties; typically less than 25 per cent, with some as low as 5 per cent for stronger lines.

4 IMPACT ON SOLAR SPECTRAL SYNTHESIS

The Sun offers an excellent test-bed for new atomic data, with its high-resolution spectrum (Kurucz et al. 1984) and accurately known fundamental parameters (US Naval Observatory & H.M. Nautical Almanac Office 2013). To assess the impact of our new $\log(gf)$ values on stellar syntheses, and also verify their general accuracy, we have determined line-by-line solar Fe abundances for a subset of 36 lines listed in Table 3 using both our new $\log(gf)$ values and the best previously published values that are not of astrophysical nature. These lines, shown in Table 5, were selected as they are blend-free at the spectral resolution of the Kitt Peak FT Spectrometer ($R \approx 200\,000$) flux atlas (Kurucz et al. 1984), and are accompanied by good broadening parameters and accurate continuum placement. The synthesis and abundance determination were performed under the assumption of local thermodynamic equilibrium (LTE), with the one-dimensional, plane-parallel radiative transfer code SME (Valenti & Piskunov 1996), using a MARCS model atmosphere (Gustafsson et al. 2008).

We adopted a solar effective temperature $T_{\text{eff}} = 5777$ K, a surface gravity $\log(\text{grav.}) = 4.44$, a microturbulence of $\xi_{\text{vmic}} = 1.0$ km s⁻¹ and a projected rotational velocity of $v_{\text{rot}} \sin(i) = 2.0$ km s⁻¹. The radial-tangential macro-turbulence velocity, ξ_{vmac} , was varied between 1.5 and 2.5 km s⁻¹ to match the observed profile. The instrumental profile was assumed to be Gaussian. The line profiles were fitted individually using χ^2 -minimization between observed and synthetic spectra and varying the iron abundance.

The results are shown in Fig. 3, where the abundances are plotted as a function of $\log(gf)$ on the standard astronomical scale.

$$\log[\epsilon(\text{Fe})] = \log_{10} \left[\frac{N(\text{Fe})}{N(\text{H})} \right] + 12, \quad (7)$$

where $N(\text{Fe})$ and $N(\text{H})$ are the number of iron and hydrogen atoms per unit volume, respectively.

Reassuringly, the new experimental data result in a small line-to-line scatter (0.08 dex)² and a mean abundance of 7.44, which is in good agreement with recent publications, such as 7.43 ± 0.02 from Bergemann et al. (2012, MARCS, LTE result). In contrast, the best previously published values (omitting the discrepant semi-empirical values shown in Fig. 3) produce an abundance of 7.49 ± 0.13 , with the significantly larger scatter driven by the lines with no previous laboratory measurements. The observed and best-fitting synthetic profiles of three of these lines are shown in Fig. 4. They all fall within the GES wavelength windows, and two of them are also in the near-infrared *Gaia* Radial Velocity Spectrometer window (Katz et al. 2004).

Other lines with significant improvements in the solar modelling, but not shown in Table 5, are those at 4079.2, 4933.9 and 5171.7 Å, which are partly blended with astrophysically interesting lines such as the Ba II 4934.0 Å line, the Mn I 4079.2 Å line and the Mg I triplet line at 5172.7 Å.

5 SUMMARY

In Table 3, we have provided new $\log(gf)$ values for 142 Fe I lines from 12 upper levels, which include 38 lines of particular interest for the analysis of stellar spectra obtained by the GES survey. Where $\log(gf)$ values existed for these lines in the literature, we have found good agreement with our new values, which in many cases have smaller experimental uncertainties than those previously reported. This is especially true for uncertainties in $\log(gf)$ values from May et al. (1974), which have been reduced from 50 per cent or more to less than 25 per cent in most cases.

This work represents part of an ongoing collaboration between IC, U. Wisconsin and NIST to provide the astronomy community with Fe I $\log(gf)$ values needed for the analysis of astrophysical spectra. Further publications will follow in the near future.

ACKNOWLEDGEMENTS

MPR and JCP would like to thank the UK Science and Technology Facilities Council (STFC) for supporting this research and the European Science Foundation (ESF), under GREAT/ESF grant number 5435, for funding international travel to discuss research plans with the wider GES team. EDH and JEL acknowledge the support of the US National Science Foundation (NSF) for funding the LIF lifetime measurements under grants AST-0907732 and AST-121105. KL acknowledges support by the European Union FP7 programme through European Research Council (ERC) grant number 320360.

Please note that the identification of commercial products in this paper does not imply recommendation or endorsement by the NIST, nor does it imply that the items identified are necessarily the best available for the purpose.

REFERENCES

- Anstee S. D., O'Mara B. J., 1991, MNRAS, 253, 549
 Anstee S. D., O'Mara B. J., 1995, MNRAS, 276, 859
 Bard A., Kock A., Kock M., 1991, A&A, 248, 315
 Bergemann M., Lind K., Collet R., Magic Z., Asplund M., 2012, MNRAS, 427, 27
 Bigot L., Thévenin F., 2006, MNRAS, 372, 609
 Blackwell D. E., Petford A. D., Shallis M. J., Simmons G. J., 1982, MNRAS, 199, 43
 Fuhr J. R., Wiese W. L., 2006, J. Phys. Chem. Ref. Data, 35, 1669
 Gilmore G. et al., 2012, The Messenger, 147, 25
 Gray D. F., 2005, The Observation and Analysis of Stellar Photospheres, 3rd edn. Cambridge Univ. Press, Cambridge, p. 231
 Gustafsson B., Edvardsson B., Eriksson K., Jørgensen U. G., Nordlund Å., Plez B., 2008, A&A, 486, 951
 Huber M. C. E., Sandeman R. J., 1986, Rep. Prog. Phys., 49, 397
 Katz D. et al., 2004, MNRAS, 354, 1223
 Kelleher D. E., Podobedova L. I., 2008, J. Phys. Chem. Ref. Data, 37, 267
 Kurucz R. L., 2007, <http://kurucz.harvard.edu/atoms/2700/>
 Kurucz R. L., Furenlid I., Brault J., Testerman L., 1984, National Solar Observatory Atlas: Solar flux atlas from 296 to 1300 nm National Solar Observatory, Sunspot, NM
 Lawler J. E., Den Hartog E. A., Sneden C., Cowan J. J., 2008, Can. J. Phys., 86, 1033
 Marek J., Richter J., Stahnke H. J., 1979, Phys. Scr., 19, 325
 May M., Richter J., Wichelmann J., 1974, A&AS, 18, 405
 Nave G., Johansson S., Learner R. C. M., Thorne A. P., Brault J. W., 1994, ApJS, 94, 221
 Nave G., Sansonetti C. J., Griesmann U., 1997, in OSA Technical Digest Ser. Vol. 3, Fourier Transform Spectroscopy. Opt. Soc. Am., Washington, DC, p. 38

² The unit dex stands for decimal exponent. x dex = 10^x .

- O'Brian T. R., Wickliffe M. E., Lawler J. E., Whaling W., Brault J. W., 1991, *J. Opt. Soc. Am. B*, 8, 1185
- Perryman M. A. C. et al., 2001, *A&A*, 369, 339
- Pickering J. C., Thorne A. P., Perez R., 2001a, *ApJS*, 132, 403
- Pickering J. C., Johansson S., Smith P. L., 2001b, *A&A*, 377, 361
- Pickering J. C., Blackwell-Whitehead R., Thorne A. P., Ruffoni M. P., Holmes C. E., 2011, *Can. J. Phys.*, 89, 387
- Ruffoni M. P., 2013, *Comput. Phys. Commun.*, 184, 1770
- Ruffoni M. P., Allende-Prieto C., Nave G., Pickering J. C., 2013, *ApJ*, 779, 17
- Thorne A. P., 1996, *Phys. Scr.*, T65, 31
- Thorne A. P., Harris C. J., Wynne-Jones I., Learner R. C. M., Cox G., 1987, *J. Phys. E*, 20, 54
- Thorne A. P., Litzén U., Johansson S., 2007, in *Spectrophysics: Principles and Applications*, 3rd edn. Springer-Verlag, Berlin, Chapter 7.7
- US Naval Observatory, H.M. Nautical Almanac Office, 2013, *The Astronomical Almanac for the Year 2014*. US Government Printing Office (USGPO), Washington, DC and The Stationery Office, London
- Valenti J. A., Piskunov N., 1996, *A&AS*, 118, 595
- Volz U., Schmoranzner H., 1998, in Mohr P. J., Wiese W. L., eds, *AIP Conf. Proc. Vol 434, Atomic and Molecular Data and Their Applications*. Am. Inst. Phys., New York, p. 67
- Yan Z.-C., Tambasco M., Drake G. W. F., 1998, *Phys. Rev. A*, 57, 1652

SUPPORTING INFORMATION

Additional Supporting Information may be found in the online version of this article:

Table 3. Experimental BFs, transition probabilities, and $\log(gf)$ for the Fe I levels listed in Table 2.

Table 4. Lines measured in previous studies, or predicted to have a BF greater than 1 per cent, that were omitted from the BF measurements shown in Table 3 (<http://mnras.oxfordjournals.org/lookup/suppl/doi:10.1093/mnras/stu780/-/DC1>).

Please note: Oxford University Press is not responsible for the content or functionality of any supporting materials supplied by the authors. Any queries (other than missing material) should be directed to the corresponding author for the paper.

This paper has been typeset from a $\text{\TeX}/\text{\LaTeX}$ file prepared by the author.